

Spreading in Integrable and Non-integrable Many-Body Systems

Johannes Freese, Boris Gutkin and Thomas Guhr

Fakultät für Physik, Universität Duisburg-Essen, Lotharstraße 1, 47048 Duisburg, Germany

(Dated: March 22, 2022)

We consider a finite, closed and selfbound many-body system in which a collective degree of freedom is excited. The redistribution of energy and momentum into a finite number of the non-collective degrees of freedom is referred to as spreading as opposed to damping in open systems. Spreading closely relates to thermalization, but while thermalization requires non-integrability, spreading can also present in integrable systems. We identify subtle features which determine the onset of spreading in an integrable model and compare the result with a non-integrable case.

PACS numbers: 05.45.Mt, 21.60.Ev

Keywords: many-body systems, collective modes, spreading, integrability

I. INTRODUCTION

Almost sixty years ago, Fermi, Pasta and Ulam [1] presented a puzzling study of a many-body system which contrary to the intuition does not thermalize: the phase space is not ergodically filled. They studied an one-dimensional chain of point particles coupled by springs with a small nonlinear force. It was found numerically that the energy which was put into the lowest Fourier mode almost completely stayed there, even after very long times, rather than being distributed over many or all modes. An understanding was achieved in a continuum limit which leads to a Korteweg-de Vries equation allowing for soliton solutions. A recent review can be found in Ref. [2]. Some years ago, Kinoshita, Wenger and Weiss [3] studied a different but related problem in a real experiment. They realized a quantum Newton's cradle by letting two one-dimensional Bose gases collide and oscillate against each other. Once more, thermalization did not take place, the two Bose gases kept their shapes even after many oscillations. Subsequently this lack of thermalization was attributed to the integrability of the problem. This conclusion however is sometimes challenged because the system is only weakly interacting and can thus be viewed as two sub-systems (the centers of mass of the two Bose gases) which collide without effect on their inner structure [4]. Thermalization and related issues are presently an active field of research, see Refs. [5, 6] and references therein. The notion of thermalization is sometimes restricted to infinite many-body systems. Here, we use it in a broader sense, including large but finite many-body systems as, for example, Bose gases and atomic nuclei.

Thermalization can be accompanied by another phenomenon – *spreading* of collective motion. It is often observed in closed (and finite) many-body systems that exhibit collective and incoherent single-particle motion simultaneously. Energy and momentum from one distinct — in the present context collective — degree of freedom is redistributed into many other single-particle degrees of freedom. This has to be distinguished from *damping* as occurring in open systems. In the latter case, the energy leaves the system because of coupling to a large or

even infinite number of external degrees of, *i.e.*, to an external bath as studied in the generic Caldeira-Leggett model [7].

Among the numerous examples for spreading of collective motion in atomic nuclei [8], the Giant Dipole Resonance, as schematically depicted in Fig. 1, is probably the most well-known one. The cross section of the electric dipole radiation as well as the spectral density of the excitations show at a certain energy a huge peak whose spreading width is orders of magnitudes larger than the mean level spacing. A simple, somehow semiclassical pic-

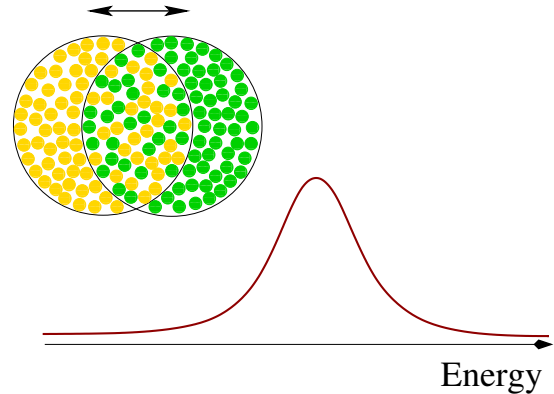


Figure 1: Schematic sketch of a Giant Dipole Resonance. The peak is the envelope of a very large number of individual quantum mechanical resonances which cannot be resolved in an experiment.

ture helps to catch the salient features of this effect: The neutrons may be viewed as confined to one sphere, the protons to another one. Relative motion of the nucleons inside these spheres does not take place. The two spheres move against each other, thereby carrying out a fully collective motion. This results in an enormous response function. A bit further away from the resonance energy, relative motion inside the spheres sets in which lowers the cross section. Much further away, all motion is incoherent of single-particle type, the motion is not collective anymore, and the resonance has disappeared completely. Besides the Giant Dipole Resonance, many other forms of collective motion and the associated spreading

exist in nuclei, see recent examples in Refs. [9, 10]. Further examples of collective motion can also be found in Bose–Einstein condensates [3, 11–13]. Here, we study an effect inspired by the Giant Dipole Resonance in a simple system of interacting particles.

As opposed to thermalization, chaos is not crucial for the presence or absence of spreading. Spreading of collective motion might occur even in integrable systems [14, 15]. However, as we show in the present study, the details of this process are very sensitive to the choice of the system parameters. In particular, we demonstrate that in the integrable case pronounce spreading occurs only for fine tuned interactions between system particles. We also study numerically how the onset of chaos influences both, collective and single–particle dynamics.

The paper is organized as follows. In Sec. II, the model is introduced and the procedure of its numerical solution are discussed. We present the results for the integrable and non–integrable cases in Secs. III and IV, respectively. We conclude in Sec. V.

II. SETUP OF THE MODEL

We largely use the model introduced in our previous analytical investigations [14, 15]. Two clouds of interacting particles in one dimension are coupled to each other. In the integrable case, all interactions between particles are harmonic. A forth–order term is added then to explore a weakly non–integrable regime. The clouds are initially separated and then released, which does or does not lead to a spreading of the initial energy and momentum over all degrees of freedom.

As we found it appropriate to slightly change some conventions of [14, 15] for the numerical study, we compile all necessary formulas defining the Hamiltonian in Sec. II A. We discuss the choice of collective coordinate in Sec. II B. The numerical method and the initial conditions are explained in the Secs. II C and II D, respectively.

A. Hamiltonian

The two clouds, labeled $a = 1, 2$, of N point particles each with equal masses m , move in one dimension. Their positions and momenta are denoted $x_i^{(a)}$, $i = 1, \dots, N$ and $p_i^{(a)}$, $i = 1, \dots, N$, respectively. The total Hamiltonian is

$$H = H_0 + \lambda H_{\text{ni}} . \quad (1)$$

The first part of H is the integrable Hamiltonian as discussed in Ref. [14],

$$H_0 = H_0^{(1)} + H_0^{(2)} + \kappa H_0^{(12)} , \quad (2)$$

where the terms

$$H_0^{(a)} = \frac{1}{2m} \sum_{i=1}^N \left(p_i^{(a)} \right)^2 + \sum_{i \neq j}^N V_{ij} \left(x_i^{(a)} - x_j^{(a)} \right)^2 , \quad (3)$$

model the two harmonic clouds $a = 1, 2$ which are coupled with the interaction term

$$H_0^{(12)} = \sum_{i,j=1}^N K_{ij} \left(x_i^{(1)} - x_j^{(2)} \right)^2 . \quad (4)$$

As already pointed out, we focus on selfbound systems. Here, we find it convenient to ensure this directly by using the translation invariant differences of the positions in Eqs. (3,4). The selfboundness is ensured since we choose both the coefficients K_{ij} , V_{ij} from symmetric $N \times N$ matrices K, V with positive entries. In contrast to Refs. [14, 15] we introduce the control parameter κ for tuning the overall strength ratio of the interactions between the clouds. Finally, the second term λH_{ni} in (1) renders the total Hamiltonian H non–integrable.

We order the positions and momenta in two $2N$ component vectors $x = (x^{(1)}, x^{(2)})$ and $p = (p^{(1)}, p^{(2)})$ with the N component vectors $x^{(a)} = (x_1^{(a)}, \dots, x_N^{(a)})$ and $p^{(a)} = (p_1^{(a)}, \dots, p_N^{(a)})$ for $a = 1, 2$. Furthermore, it is helpful to cast the integrable case for $\lambda = 0$ into a more compact form. Defining the $2N \times 2N$ positive, symmetric interaction matrix

$$C = \begin{bmatrix} W & -\kappa K/2 \\ -\kappa K/2 & W \end{bmatrix} , \quad (5)$$

with

$$W_{ij} = \left(2 \sum_{l=1}^N V_{il} + \kappa K_{il} \right) \delta_{ij} - V_{ij} , \quad (6)$$

the potential becomes a standard bilinear form and we arrive at the expression

$$H_0 = \frac{p^2}{2m} + x^T C x . \quad (7)$$

To fix the notation, we write down the elementary transformation to normal modes explicitly. An orthogonal matrix U diagonalizes the interaction matrix,

$$C = \frac{m}{2} U^T \omega^2 U$$

$$\omega = \text{diag}(\omega_1, \dots, \omega_{2N}) , \quad (8)$$

where the eigenvalues $m\omega_i^2/2$, $i = 1, \dots, 2N$ of C are non–negative, because the matrices V and K have positive entries. In the rotated coordinates

$$\xi = Ux \quad \text{and} \quad \pi = Up \quad (9)$$

the system Hamiltonian decouples into $2N$ non–interacting ones,

$$H_0 = \sum_{i=1}^{2N} \left(\frac{\pi_i^2}{2m} + \frac{1}{2} m \omega_i^2 \xi_i^2 \right) . \quad (10)$$

The positive quantities ω_i are of course the system eigenfrequencies. The coordinates ξ_i and π_i are not positions and momenta of the particles, rather they are

weighted linear combinations and can be viewed as positions and momenta of the non-interacting composite particles which define the normal modes. The transformation (10) also facilitates an elementary solution of the equations of motions, allowing for a crucial check of our numerics later on.

In Ref. [15], we extended the integrable model (2) by adding a rather general translation invariant term which breaks the integrability but preserves the selfboundness. For our numerical study we make the special choice λH_{ni} with a strength parameter λ and the fourth-order potential

$$H_{\text{ni}} = \sum_{i,j=1}^N P_{ij} \left(x_i^{(1)} - x_j^{(2)} \right)^4 . \quad (11)$$

The coefficients P_{ij} are as well taken from a symmetric $N \times N$ matrix P with positive entries. This non-integrable interaction preserves translation invariance and selfboundness.

B. Collective Coordinate

We aim at studying the interplay between collective and incoherent single-particle motion. Many-body systems show a rich variety of collective excitations, particularly nuclei provide a zoo of examples [8]. Of course the way how the system is probed determines which collective modes are excited. As we have in mind excitation in which the two clouds are simply pulled apart and then released to oscillate against each other, the natural choice for the collective coordinate in our case is the difference of the centers of mass in each cloud

$$\Xi = \frac{1}{N} \sum_{i=1}^N x_i^{(1)} - \frac{1}{N} \sum_{i=1}^N x_i^{(2)} . \quad (12)$$

Although this definition is fully equivalent to the one we used previously, we notice that the collective coordinate X in Ref. [15] differs by a factor, *i.e.*, we have $\Xi = \sqrt{N}/2X$. The time evolution $\Xi(t)$ of the collective coordinate is our most important observable. The larger the typical amplitudes $|\Xi(t)|$ of the collective motion after some time t , the more of energy and momentum is contained in the oscillation between the two clouds. The smaller the amplitudes, the more of energy and momentum is transferred to the incoherent single-particle degrees of freedom within the clouds.

C. Numerical Solution

For the numerical integration of the equations of motion we found it efficient to use the Velocity Verlet Method, see *e.g.* Ref. [16], a standard method in molecular dynamics. We employed various well-established techniques and tests to implement it in an optimal way

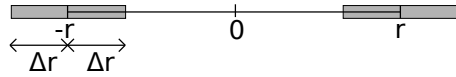


Figure 2: The initial positions of the particles are randomly chosen within the shaded intervals.

for our system. In particular, we carefully checked that the energy is conserved even for very long times beyond those we were interested in. As already mentioned in Sec. II A, we compared the exact solution of the integrable model with a direct numerical integration which turned out highly useful to eliminate even subtle errors. To further test the results of our simulation we validated that our numerical simulation remains stable under time reversal transformation.

D. Initial Conditions

The initial conditions are chosen such that the two clouds are separated and at rest at time $t = 0$. The initial particle positions $x_{i0}^{(1)} = x_i^{(1)}(0)$, $x_{i0}^{(2)} = x_i^{(2)}(0)$, $i = 1, \dots, N$ are taken from two uniform random distributions around some points, r and $-r$, within the intervals $[r - \Delta r, r + \Delta r]$ and $[(-r) - \Delta r, (-r) + \Delta r]$, respectively. This is illustrated in Fig. 2. In all our investigations, we used mirrored initial conditions, *i.e.*, the symmetry $x_{i0}^{(2)} = -x_{i0}^{(1)}$, $i = 1, \dots, N$. The initial particle momenta $p_{i0}^{(1)}$, $p_{i0}^{(2)}$, $i = 1, \dots, N$ are always set to zero when we investigate the integrable case in Sec. III. Only in the non-integrable case to be discussed in Sec. IV, we work with non-zero initial momenta, preserving the mirror symmetry.

III. INTEGRABLE CASE

We begin by demonstrating in Sec. III A the presence and absence of spreading in the integrable case. In Sec. III B, we give a first explanation by looking at eigenfrequencies and normal modes. We study the influence of the standard deviations of the distributions for the interaction matrix elements and of the particle number in Secs. III C and III D, respectively.

A. Presence and Absence of Spreading

We choose the entries of the interaction matrices W and K from independent Gaussian distributions with means $\langle W \rangle$, $\langle K \rangle$ and standard deviations σ_W , σ_K , respectively. The mass of each particle is always set to be 1 kg. Other parameters for numerical simulations are given in Tab. I.

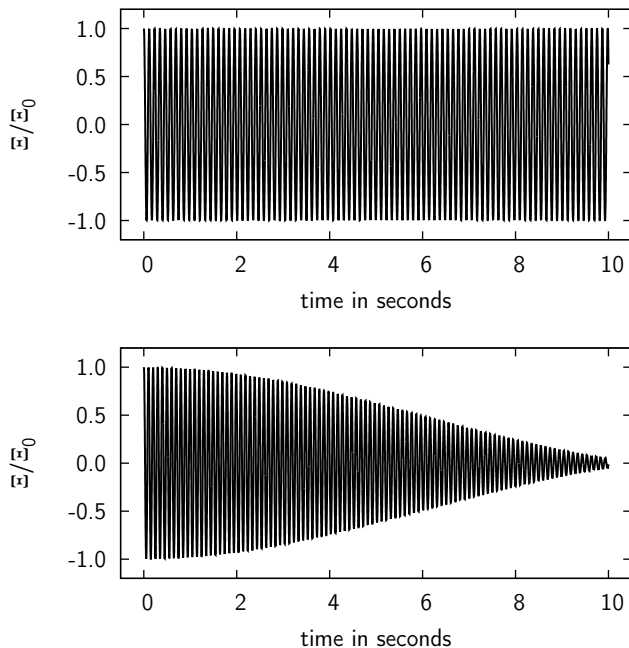


Figure 3: The ratio of collective coordinate to its initial value for $\kappa = 0.75$ (top) and $\kappa = 1.0$ (bottom) versus time from 0 to 10 seconds.

N	T	Δt	$\langle W \rangle$	σ_W
500	30 s	0.001 s	4 J/m ²	0.63 J/m ²
$\langle K \rangle$		σ_K	$ r $	Δr
2 J/m ²		0.48 J/m ²	2 m	0.2 m

Table I: Parameter set for the integrable case.

The parameter κ defining the strength ratio of the interaction within and between the clouds is still to be fixed. In Fig. 3, the collective coordinate is shown for two different values of κ . Here and in all other figures, the collective coordinates $\Xi(t)$ are normalized to their initial values Ξ_0 . As seen in Fig. 3, the results differ drastically – for $\kappa = 0.75$, the energy stays in the collective oscillation, while it is spread over the other degrees of freedom for $\kappa = 1.0$. It is instructive to plot the envelopes of the collective coordinate, this is done in Fig. 4 for four values of κ . Surprisingly, the transition from weak to almost complete spreading happens within a relatively small interval of 0.03 or so in the parameter κ . If κ is increased beyond $\kappa = 1.0$, the spreading becomes weaker again.

B. Eigenfrequencies and Normal Modes

The above results can be explained by the structure of the interaction matrix. As the eigenfrequencies (8) completely determine the interaction, we display their spectra for two values of κ in Fig. 5. We notice that half

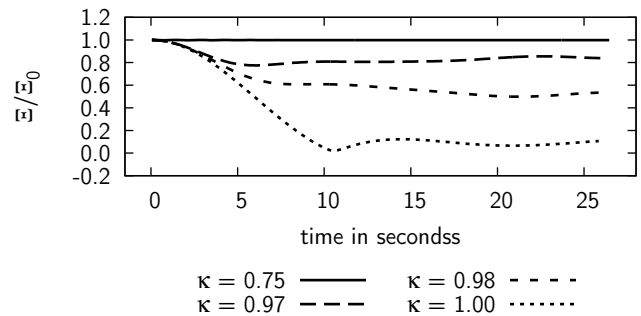


Figure 4: Envelope of the collective coordinate for four values of κ versus time from 0 to 10 seconds.

of the eigenfrequencies are not excited, which is due to the mirrored initial conditions. This symmetry causes the projection to the antisymmetric eigenvectors to vanish. If using non-mirrored initial conditions, any energy stored in the corresponding degrees of freedom is completely decoupled from the collective coordinate. Hence, it does not have an effect on the dynamics of the collective coordinate. Accordingly, these frequencies are not shown in Fig. 5.

Although both spectra for $\kappa = 1$ and $\kappa = 0.98$ show broad bulks of non-degenerate eigenfrequencies, they are distinctly different. The one for $\kappa = 1$ has an isolated eigenfrequency left of the bulk. It is found to belong to the eigenvector that is close to the “collective” vector e , *i.e.*, the one where the modulus of all entries is equal, but the signs differ for the two clouds.

A general equation for the time evolution of the collective coordinate $\Xi(t)$ can be easily written down by using eigenvectors c_i $i = 1, \dots, N$ of the interaction matrix C :

$$\Xi(t) = \sum_{i=1}^N a_i \cos(\omega_i t), \quad (13)$$

where $a_i = (e, c_i)(c_i, x_0)$ and the two scalar products correspond to the projection of the eigenmode c_i on the “collective” vector and the initial state, respectively. Note that, since the initial state x_0 is always taken to be close to (a scaled) vector e (see fig. 2), both scalar products are similarly distributed. So the crucial information on the dynamics of $\Xi(t)$ can be extracted from the distribution of the initial excitations $\xi_{i0} = (c_i, x_0)$. In Fig. 6, we display the excitation of the normal modes for four different values of κ . As there is a one-to-one correspondence between the amplitude ξ_{i0} and the eigenfrequency ω_i , we show the initial amplitudes ξ_{i0} versus the eigenfrequencies ω_i to directly visualize which eigenmode is excited. Comparing with Fig. 4, we see that spreading is obviously absent if only the collective excitation is excited, whereas a broader excitation of other eigenmodes leads to spreading. The truly amazing observation is the subtlety of this process which takes place within a 3% change of

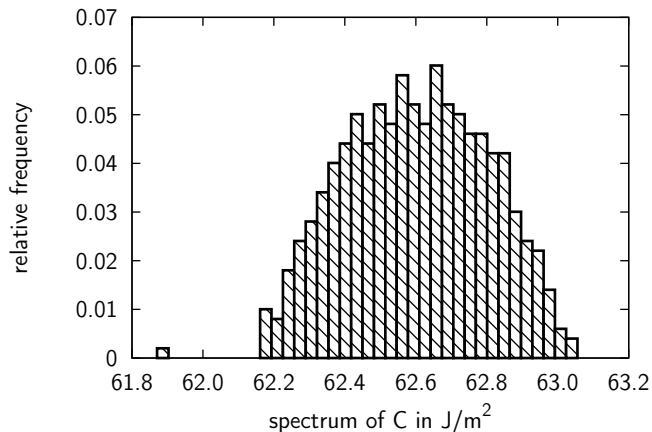
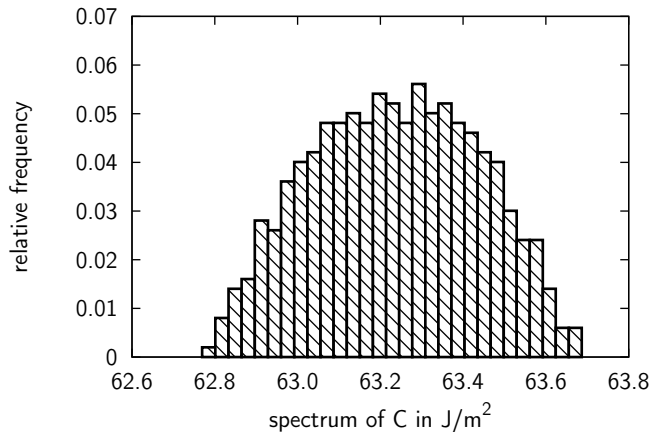


Figure 5: Spectrum of system eigenfrequencies for $\kappa = 1$ (top) and $\kappa = 0.98$ (bottom).

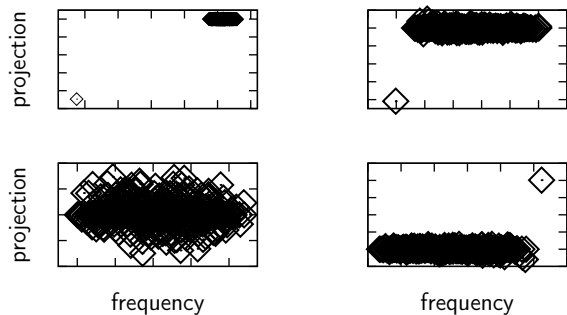


Figure 6: Excitation of the normal modes for $\kappa = 0.75, 0.97$ (top) and $\kappa = 1.0, 1.02$ (bottom) versus the eigenfrequencies.

the parameter κ and is thus due to minor changes in the structure of the interaction. We also conclude that the isolation of the eigenfrequency corresponding to the collective coordinate is essential to prevent spreading. This is seen in Fig. 6 for $\kappa = 1.02$. The crucial eigenfrequency now shows up on the right hand side of the spectral bulk.

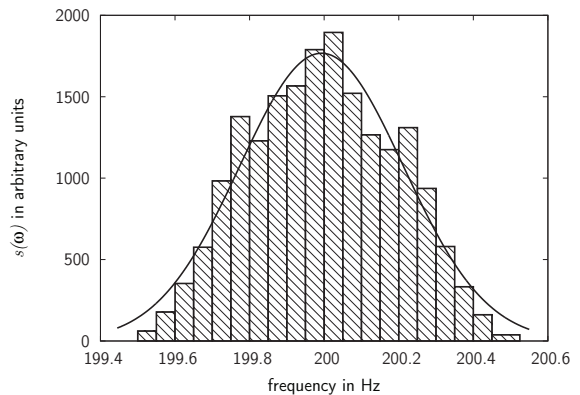


Figure 7: The figure shows a Gaussian fit of $s(w)$ for $N = 5000$ particles. Other parameters of the model are the same as in Tab. II.

As a function of κ it wandered through the bulk, it is isolated again, leading to a suppression of spreading.

If no isolated eigenvalues are present, the dynamical evolution of the collective coordinate can be estimated by eq. 13 with a smooth approximation to the spectral density $s(\omega') = \sum_{i=1}^N a_i \delta(\omega' - \omega_i)$, as a function of the continuous variable ω' ,

$$\begin{aligned} \Xi(t) &= \int_{-\infty}^{+\infty} d\omega' \cos(\omega't) \sum_{i=1}^N a_i \delta(\omega' - \omega_i) \\ &\simeq \int_{-\infty}^{+\infty} d\omega' \cos(\omega't) s(\omega'). \end{aligned} \quad (14)$$

This amounts to a Fourier transform of the spectral density. As we choose the interaction matrix elements from Gaussian distributions, it is not too surprising that a Gaussian with mean μ and width γ approximates the spectral density well, see fig. 7,

$$\begin{aligned} \Xi(t) &\sim \int_{-\infty}^{+\infty} d\omega' \cos(\omega't) \exp\left(-\frac{(\omega' - \mu)^2}{2\gamma^2}\right) \\ &\sim \exp\left(-\frac{\gamma^2 t^2}{2}\right) \cos(\mu t), \end{aligned} \quad (15)$$

leading to the Gaussian decay of the collective coordinate with the oscillation period $2\pi/\mu$ and the decay time given by $1/\gamma$. The standard deviations σ_W and σ_K in turn determine the width γ of the spectral density.

C. Modifying the Standard Deviations of the Interactions

We further investigate the remarkable sensitivity of spreading to slight variations of the interaction matrices W and K . In view of its high dimension, we refrain

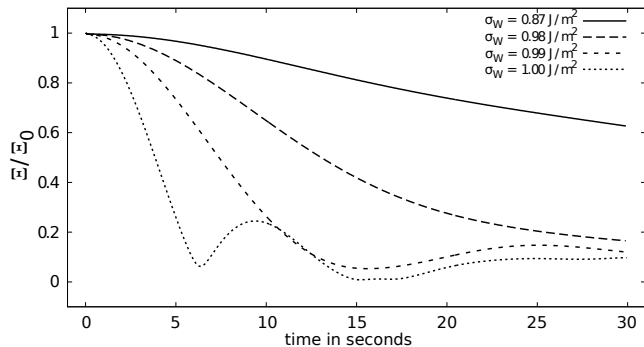


Figure 8: Envelopes of the collective coordinates versus time for four different values of σ_W .

from trying to explore the space of the interaction parameters systematically. We rather focus on some examples in which we modify the standard deviations σ_W and σ_K of the probability distributions for the elements of the interaction matrices W and K . The parameters for these numerical simulations are given in Tab. II.

N	T	Δt	$\langle W \rangle$	$\langle K \rangle$	r	Δr
500	30 s	0.001 s	2 J/m ²	1 J/m ²	2 m	0.2 m

Table II: Parameter set for the test of the standard deviation dependence.

We notice that the relative strength parameter is now fixed to $\kappa = 2$. Furthermore, we found it convenient to keep the standard deviation of the interaction between the clouds constant, $\sigma_K = 0.1$, and only to vary the standard deviation σ_W of the interaction within the clouds. In Fig. 8, the envelopes of the collective coordinates are shown for four values of σ_W . The smaller the standard deviation σ_W , the narrower the distribution of the eigenfrequencies, resulting in the system being less likely to show spreading. Again, it is surprising that even relatively small changes in σ_W have a strong impact. This behavior remains the same, if σ_K is changed and σ_W is held fixed.

D. Dependence on the Particle Number

One is tempted to expect, based on observations in statistical mechanics, that the number of particle itself is important for the decay of the collective coordinate: the larger the number of degrees of freedom, the larger the recurrence times and the more effective ought to be the process of thermalization. Accordingly, a large particle number should make spreading more efficient, and the position of the bottleneck should decrease with the number of particles. In Fig. IIID, however, we see a different behavior. The parameters for these numerical simulations are listed in Tab. III.

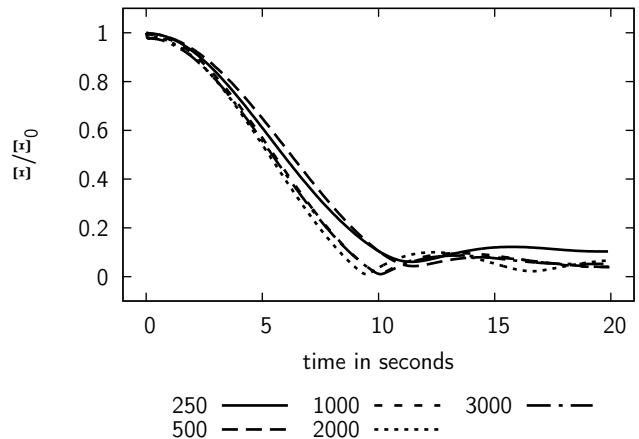


Figure 9: Envelopes of the collective coordinates versus time for five different particle numbers N .

T	Δt	$\langle W \rangle$	$\langle K \rangle$	r	Δr
3 s	0.001 s	4 J/m ²	2 J/m ²	2 m	0.2 m

Table III: Parameter set for the particle number dependence

The number of particles N strongly affects the local timescales, resulting in ever faster oscillations when N grows. This is so because the total mass of the system increases linearly with N , while the number of interactions for a given particle with other particles goes with N^2 . Hence, the oscillations periods decrease. As argued above, the global timescale for the spreading depends on the standard deviations of the interactions. For the present choice of parameters, these means that the decay time and thus position of the bottleneck is roughly the same for all particle numbers. However, another expectation from statistical mechanics manifests itself in these simulations. As Fig. 10 illustrates, the bottleneck becomes sharper with increasing particle number.

IV. NON-INTEGRABLE CASE

In Sec. IV A, we investigate and compare non-integrable perturbations of different strengths, before we take a closer look at the trajectories in the phase space by slightly varying the initial conditions in Sec. IV B.

A. Perturbations of Different Strengths

We use the full Hamiltonian (1) with the non-integrable part (11). The interaction matrices W and K for the integrable harmonic interaction, the parameter κ , as well as the interaction matrix P for the non-integrable

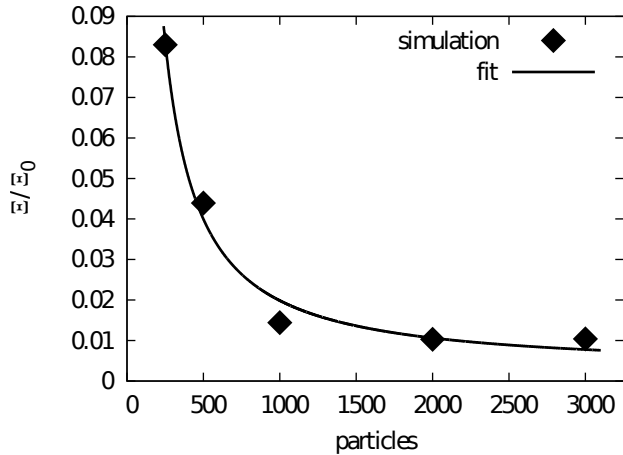


Figure 10: Normalized amplitude of the collective coordinate at the bottleneck position versus particle number N .

perturbation are kept fixed in all simulations to be presented here. The parameters are given in Tab. IV.

N	T	Δt	$\langle w \rangle$	v_w	$\langle k \rangle$	v_k
500	20 s	0.0005 s	2 J/m ²	0.2 J/m ²	1 J/m ²	0.1 J/m ²
			$\langle P \rangle$	v_P	r	Δr
			1.5 J/m ²	0.15 J/m ²	2 m	0.2 m
					Δv	
					0.0001 m/s	

Table IV: Parameter set for the investigation of the perturbation influence.

Only the parameter λ is varied to investigate the impact of different perturbation strengths. The results of the simulations are displayed in Fig. 11. For reference, the integrable case corresponding to $\lambda = 0$ is also shown. Obviously, the non-integrability helps the spreading considerably: for the strongest perturbation, the bottleneck is reached much quicker than in all previous simulations. However, as we demonstrated in Sec. III, non-integrability is not a necessary condition for spreading.

B. Slight Variations of Initial Conditions

High sensitivity of the trajectories to slight changes in the initial conditions is the prime signature of classical chaos [17]. The proper measure is the Lyapunov exponent. In this spirit, we now measure the distance between system trajectories which differ only slightly in the initial conditions. We look at the collective coordinate as well as on some single-particle trajectories. When varying the initial conditions, we ensure that the total energy of the system remains unchanged to carry out a comparison on equal footing. To this end, we realized the changes in the initial conditions by modifying the particle momenta instead of the particle positions. We recall that in the above integrable case, the initial momenta were always

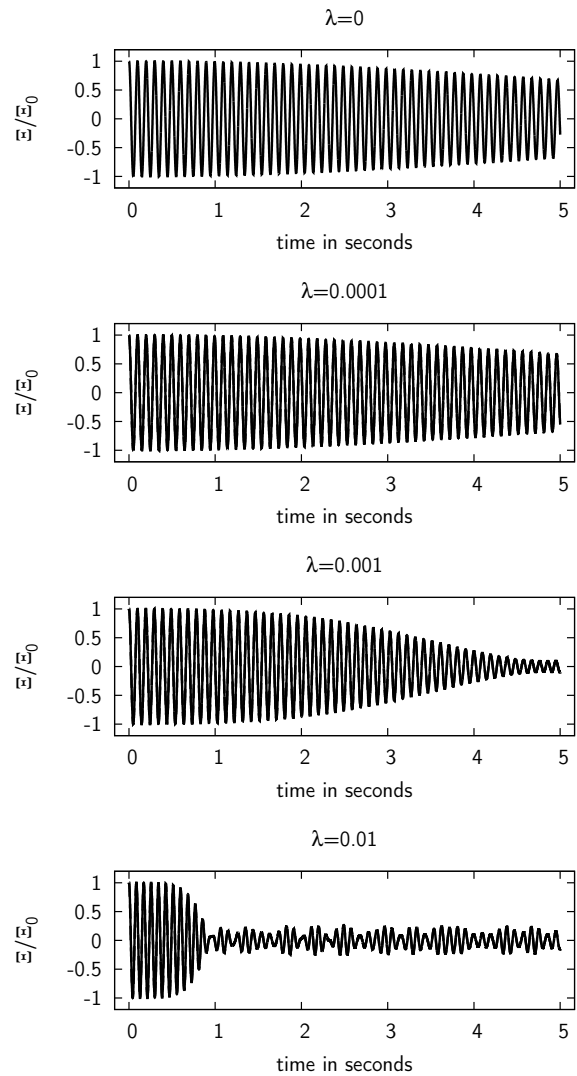


Figure 11: Collective coordinates for different strength λ of the non-integrable perturbation.

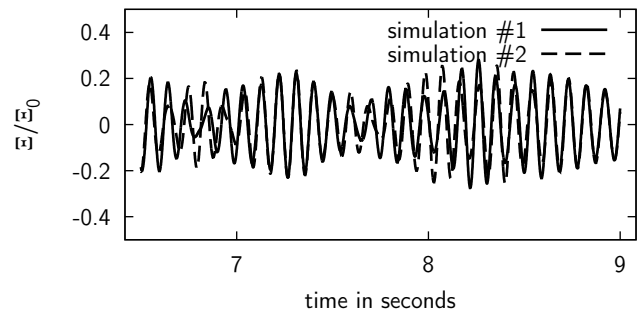


Figure 12: Collective coordinate for $\lambda = 10^{-2}$ at larger times. The ordinate is different from the one in Fig. 11 where the short-time behavior is shown.

zero. Here, in the non-integrable case, one randomly chosen particle is given a fixed momentum pointing towards the origin. To preserve the mirror symmetry of the system, the same momentum in opposite direction is given to the corresponding particle of the second cloud.

As follows from Fig. 11, there is a considerable impact of the perturbation on the spreading. This means, energy and momentum must be redistributed to the incoherent, *i.e.*, non-collective, degrees of freedom, because the amplitude of the collective coordinate decreases the faster the stronger the perturbation. Nevertheless, we expect the motion of the collective coordinate to remain largely regular [15] on local time scales. To further investigate this, we look at the strongest perturbation with $\lambda = 10^{-2}$. We compare simulations with slightly different initial conditions. In Fig. IV A, are plotted the collective coordinates for larger times, beyond the time scale displayed in Fig. 11. The first deviations are seen in the region starting at about 6.5 s. The two curves collapse then on top of each other again, before they depart once more at about 7.5 s. This confirms that the motion of the collective coordinate remains largely regular.

To better visualize individual trajectories, we go to two spatial dimensions by adding the same Hamiltonian that we use for positions and momenta in x direction also for a new set of positions and momenta in y direction. The motions in these two direction are thus uncoupled. As compared to the collective motion, the single-particle trajectories show a much stronger onset of chaotic motion, as demonstrated in Fig. 13. Here, the differences in the initial conditions can directly be read off from the figure. The two trajectories are iterated for 10 s. At short times close to 0 s, they differ only little, but at about 10 s the trajectories are completely apart. Roughly speaking, the effects due to perturbation accumulate at later times.

V. CONCLUSIONS

Thermalization in a narrower sense refers to systems of infinitely many particles. Among others features, infinite systems have the advantage of infinite recurrence times, at least in non-integrable cases. Nevertheless, the concepts of spreading in closed and of damping in open *finite* many-body systems are intimately related to thermalization. They are of high practical relevance, since there is a wealth of such systems, particularly nuclei, atoms, molecules and Bose-Einstein condensates. In parts of the literature, spreading, damping and thermalization are not clearly distinguished, and the term thermalization is often used as some kind of hypernym.

We studied spreading in a closed, selfbound many-body system for particle numbers large enough to ensure that the recurrence times did not play a role. Our first result is a clarification: the phenomenon of spreading is not tied to chaotic motion. We clearly showed that integrable systems can exhibit spreading. Thus, chaos is not a necessary prerequisite. Thermalization, however,

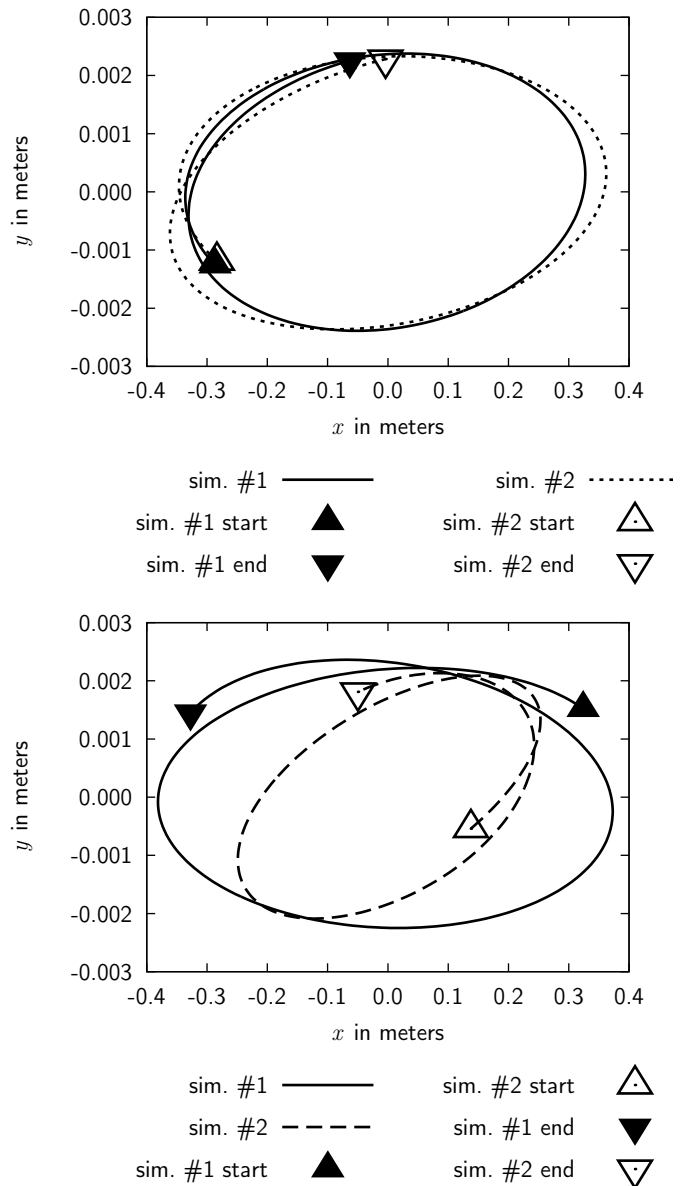


Figure 13: Single-particle trajectories with slightly different initial conditions in the two-dimensional position space for $\lambda = 10^{-2}$ followed for 0.125 s, at shorter times close to 0 s (top) and at larger times of about 10 s (bottom). We notice a factor of 100 between the scales of the x and y direction. The beginning and the end of the trajectories are marked with triangles, pointing upwards and downwards, respectively. Filled and open triangles correspond to the two different trajectories.

always requires non-integrability. Our second main result is the subtlety of the effects. Minor modifications in the relative strength parameters or in the distributions of interaction matrix elements can have a large impact. The particle number does not necessarily change the time scale on which spreading occurs. We explained this by discussing the role of eigenfrequencies and normal modes.

The details of the interactions are crucial, a normal mode corresponding to the collective coordinate in question has to exist and has to be isolated from the other eigenfrequencies and, obviously, it must be excited by the initial conditions.

Finally, non-integrability, *i.e.*, the onset of chaotic motion can considerably accelerate spreading. Our third main result is the different behavior of the collective coordinate and of the single particles. In accordance with our earlier analytical findings, the former continues to move in a largely regular fashion, while the single parti-

cles show the onset of chaoticity much stronger.

Acknowledgements

We thank Jens Hämmerling and Sophia Schäfer for fruitful discussions. We acknowledge support from Deutsche Forschungsgemeinschaft within the Sonderforschungsbereich Transregio 12.

-
- [1] E. Fermi, J. Pasta and S. Ulam, *Studies of Nonlinear Problems*, Los Alamos Document LA-1940 (1955)
 - [2] G.P. Berman and F.M. Izrailev, *Chaos* **15**, 015104 (2005)
 - [3] T. Kinoshita, T. Wenger and D.S. Weiss, *Nature* **440**, 900 (2006)
 - [4] K. Rzażewski, private communication, Duisburg-Essen (2012)
 - [5] F.H.L. Essler, S. Kehrein, S.R. Manmana, and N.J. Robinson, *Phys. Rev.* **B89**, 165104 (2014)
 - [6] J.G. Cosme, *Phys. Rev.* **A92**, 033607 (2015)
 - [7] A. O. Caldeira and A. J. Leggett, *Physica* **A121**, 587 (1983)
 - [8] A. Bohr and B. Mottelson, *Nuclear Structure, Vols. 1 and 2*, W.A. Benjamin (1969)
 - [9] J. Enders, T. Guhr, N. Huxel, P. von Neumann-Cosel, C. Rangacharyulu and A. Richter, *Phys. Lett.* **B486**, 273 (2000)
 - [10] J. Enders, T. Guhr, A. Heine, P. von Neumann-Cosel, V.Y. Ponomarev, A. Richter and J. Wambach, *Nucl. Phys.* **A741**, 3 (2004)
 - [11] D.A. Butts and D.S. Rokhsar, *Nature* **397**, 327 (1999)
 - [12] K.W. Madison, F. Chevy, W. Wohlleben and J. Dalibard, *Phys. Rev. Lett.* **84**, 806 (2000)
 - [13] O.M. Marago, S.A. Hopkins, J. Arlt, E. Hodby, G. Hechenblaikner and C.J. Foot, *Phys. Rev. Lett.* **84**, 2056 (2000)
 - [14] J. Hämmerling, B. Gutkin and T. Guhr, *J. Phys.* **A43**, 265101 (2010)
 - [15] J. Hämmerling, B. Gutkin and T. Guhr, *Eur. Phys. Lett.* **96**, 20007 (2011)
 - [16] A. Hinchliffe, *Molecular Modelling for Beginners*, 2nd edition, John Wiley & Sons (2008)
 - [17] M. C. Gutzwiller, *Chaos in Classical and Quantum Mechanics*, Springer Verlag, New York (1990)